

# Unusual superexchange pathways in a Ni triangular lattice of $\text{NiGa}_2\text{S}_4$ with negative charge-transfer energy

K. Takubo, T. Mizokawa, and J.-Y. Son

*Department of Physics & Department of Complexity Science and Engineering,  
University of Tokyo, Chiba 277-8561, Japan*

Y. Nambu and Y. Maeno

*Department of Physics, Kyoto University, Kyoto 606-8502, Japan*

S. Nakatsuji

*Department of Physics, Kyoto University, Kyoto 606-8502, Japan and  
Institute for Solid State Physics, University of Tokyo, Chiba 277-8581, Japan*

(Dated: November 12, 2018)

## Abstract

We have studied the electronic structure of the Ni triangular lattice in  $\text{NiGa}_2\text{S}_4$  using photoemission spectroscopy and subsequent model calculations. The cluster-model analysis of the Ni  $2p$  core-level spectrum shows that the S  $3p$  to Ni  $3d$  charge-transfer energy is  $\sim -1$  eV and the ground state is dominated by the  $d^9L$  configuration ( $L$  is a S  $3p$  hole). Cell perturbation analysis for the  $\text{NiS}_2$  triangular lattice indicates that the strong S  $3p$  hole character of the ground state provides the enhanced superexchange interaction between the third nearest neighbor sites.

PACS numbers: 75.30.Et, 79.60.-i, 75.50.-y

Unusual magnetic properties of geometrically frustrated spin systems have been attracting broad interest of many theorists and experimentalists in the field of condensed matter physics [1]. In frustrated spin systems with orbital degeneracy, specific orbital patterns can lift the magnetic frustration and some long range magnetic orderings can be realized in the ground state [2, 3, 4, 5, 6]. In frustrated spin systems without orbital degeneracy, spin-lattice coupling tends to provide cooperative distortion lifting the magnetic frustration [7, 8, 9] or small randomness tends to induce spin freezing at low temperature [10]. Therefore, although spin disordered states including the resonating-valence bond state are expected in the geometrically frustrated spin systems [11, 12], few systems show spin disordered states as ground states [13]. Among the various magnetic compounds with geometrically frustrated lattice, the newly-discovered NiGa<sub>2</sub>S<sub>4</sub> has the Ni<sup>2+</sup> ( $S=1$ ) triangular lattice layer without orbital degeneracy (see Fig. 1) and is found to have a spin disordered ground state using neutron diffraction experiment [14]. The neutron result also indicates that the spin-spin correlation between the third nearest neighbors is much stronger than that between the first and second nearest neighbors, indicating that the conventional triangular lattice model with the nearest neighbor superexchange coupling is not enough to describe NiGa<sub>2</sub>S<sub>4</sub> [15].

In order to understand the origin of the unusual magnetic properties of NiGa<sub>2</sub>S<sub>4</sub>, it is highly important to reveal its underlying electronic structure. In this Letter, we report photoemission study of NiGa<sub>2</sub>S<sub>4</sub> single crystals. The photoemission results and subsequent model calculations indicate that the ground state has the  $d^9L$  character ( $L$  is a S  $3p$  hole) and that the strong S  $3p$  hole character of the ground state provides the enhanced superexchange interaction between the third nearest neighbor sites. NiGa<sub>2</sub>S<sub>4</sub> is a unique spin-disordered system in that the negative charge-transfer energy allows relatively long superexchange pathways.

Single crystals of NiGa<sub>2</sub>S<sub>4</sub> are grown by chemical vapor transport as described in ref. [16]. The x-ray photoemission spectroscopy measurements were performed using a JPS 9200 spectrometer equipped with a monochromatized Al  $K\alpha$  x-ray source ( $h\nu = 1486.6$  eV). The total energy resolution was  $\sim 0.6$  eV. The single crystals were cleaved *in situ* in order to obtain clean surfaces. All photoemission data were collected at room temperature within 48 hours after cleaving. As expected from the layered structure of NiGa<sub>2</sub>S<sub>4</sub>, the obtained surfaces were extremely clean and stable: the photoemission spectra were consistent with the stoichiometric surface and did not show any change during the experiment.

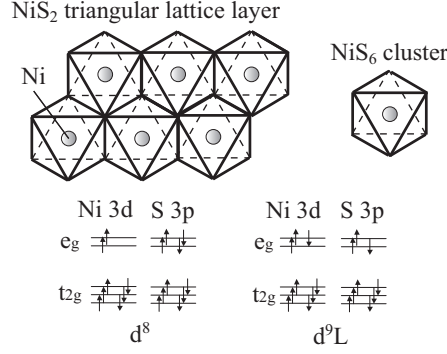


FIG. 1: Schematic drawing for the Ni<sup>2+</sup> ( $S=1$ ) triangular lattice layer and the electronic configurations of the NiS<sub>6</sub> cluster model used to analyze the photoemission spectra. The NiS<sub>2</sub> layer is constructed from the NiS<sub>6</sub> octahedra in which one Ni ion is located at the center and six S ions at the vertices. In the NiS<sub>6</sub> cluster, the S 3p molecular orbitals with  $e_g$  and  $t_{2g}$  symmetry hybridize with the Ni 3d orbitals with  $e_g$  and  $t_{2g}$  symmetry.  $L$  denotes a hole in the S 3p molecular orbitals. The charge-transfer energy  $\Delta$  is given by the excitation energy from  $d^8$  to  $d^9L$ .

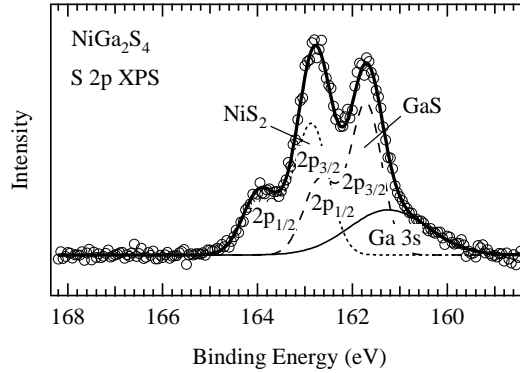


FIG. 2: S 2p and Ga 3s core-level XPS of NiGa<sub>2</sub>S<sub>4</sub> (open circles). The spectrum is fitted to five Gaussians: the Ga 3s component (thin solid curve), the  $2p_{3/2}$  and  $2p_{1/2}$  components of the GaS layer (dashed curve), and those of the NiS<sub>2</sub> layer (dotted curve). The fitted result is shown by the thick solid curve.

The S 2p core-level photoemission spectrum of NiGa<sub>2</sub>S<sub>4</sub> is shown in Fig. 2. The S 2p spectrum can be decomposed into four components: the  $2p_{3/2}$  and  $2p_{1/2}$  components of the GaS layer and those of the NiS<sub>2</sub> layer. The S 2p peaks of the NiS<sub>2</sub> layer are higher in binding energy than those of the GaS layer. The energy difference of  $\sim 1$  eV indicates that

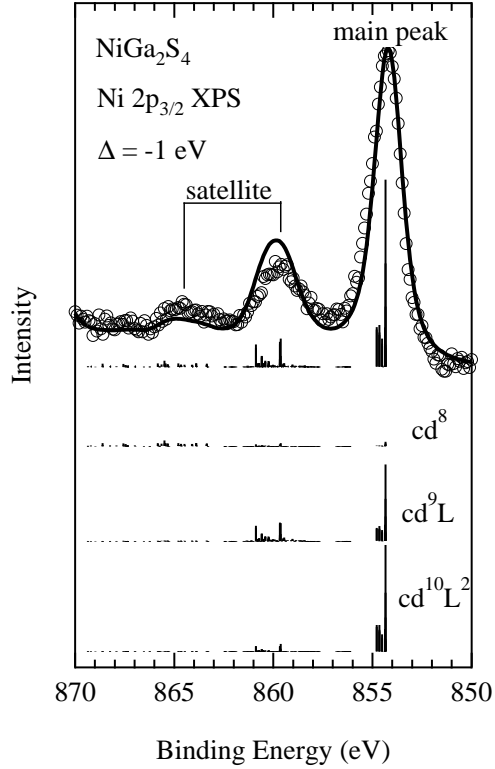


FIG. 3: Ni  $2p$  core-level XPS of  $\text{NiGa}_2\text{S}_4$  (open circles). The calculated line spectrum is broadened (solid curve) and is compared with the experimental result. In the lower panel, the line spectrum is decomposed into the  $cd^8$ ,  $cd^9L$ , and  $cd^{10}L^2$  components.

the S ions in the  $\text{NiS}_2$  layer have less valence (S  $3p$ ) electrons than those in the GaS layer. This observation already suggests that the amount of the S  $3p$  holes in the  $\text{NiS}_2$  layer is substantial as revealed by the Ni  $2p$  spectrum in the next paragraph.

The Ni  $2p$  core-level spectrum of  $\text{NiGa}_2\text{S}_4$  is shown in Fig. 3. The Ni  $2p_{3/2}$  spectrum consists of three structures: the main peak at  $\sim 854$  eV and the satellite structures at  $\sim 859$  eV and  $864$  eV. In order to extract the electronic structure parameters such as the S  $3p$  to Ni  $3d$  charge-transfer energy  $\Delta$ , the Coulomb interaction between the Ni  $3d$  electrons  $U$ , and the transfer integrals between the S  $3p$  and Ni  $3d$  orbitals ( $pd\sigma$ ), we have performed configuration-interaction calculations using an octahedral  $\text{NiS}_6$  cluster model (see Fig. 1). Since the  $\text{NiS}_6$  octahedra form the  $\text{NiS}_2$  layer sharing their edges, the interaction between the neighboring  $\text{NiS}_6$  octahedra via the S  $3p_\sigma$  orbitals pointing to the Ni sites is rather weak compared to that in the corner sharing case [17]. Therefore, the cluster-model analysis is

expected to give a good description of the Ni  $2p$  core-level spectrum. In the present cluster model, the Coulomb interaction between the Ni  $3d$  electrons are given by the Slater integrals  $F^0(3d, 3d)$ ,  $F^2(3d, 3d)$ , and  $F^4(3d, 3d)$ . The average Ni  $3d$ -Ni  $3d$  Coulomb interaction  $U$  is expressed by  $F^0(3d, 3d)$  and is an adjustable parameter.  $F^2(3d, 3d)$  and  $F^4(3d, 3d)$  are fixed to 80% of the atomic Hartree-Fock values [18]. The Coulomb interaction between the Ni  $2p$  core hole and the Ni  $3d$  electron is expressed by the Slater integrals  $F^0(2p, 3d)$ ,  $F^2(2p, 3d)$ , and  $G^1(2p, 3d)$ . The average Ni  $2p$ -Ni  $3d$  Coulomb interaction  $Q$  is expressed by  $F^0(2p, 3d)$  and is fixed to  $U/0.8$  [19, 20].  $F^2(2p, 3d)$  and  $G^1(2p, 3d)$  are fixed to 80% of the atomic Hartree-Fock values [18].

In Fig. 3, the calculated line spectrum is broadened and compared with the experimental result. The three-peak structure of the Ni  $2p_{3/2}$  spectrum is well reproduced by the calculation using  $\Delta=-1.0$  eV,  $U=5.0$  eV, and  $(pd\sigma)=-1.0$  eV. The ground state is given by the linear combination of  $d^8$ ,  $d^9L$ , and  $d^{10}L^2$  configurations:

$$\Psi_g = \alpha|d^8\rangle + \beta|d^9L\rangle + \gamma|d^{10}L^2\rangle, \quad (1)$$

where  $L$  denotes a hole in the S  $3p$  orbitals. The final states are given by the linear combinations of  $cd^8$ ,  $cd^9L$ , and  $cd^{10}L^2$  configurations, where  $c$  denotes a Ni  $2p$  core hole. In the final states, the Coulomb interaction between the Ni  $2p$  core hole and Ni  $3d$  electrons stabilizes  $cd^{10}L^2$  compared with  $cd^9L$ . The present analysis gives  $\alpha^2 = 0.25$ ,  $\beta^2 = 0.60$ , and  $\gamma^2 = 0.15$ , and the ground state is dominated by the  $d^9L$  configuration. Negative charge-transfer energy compounds have been found in some transition-metal oxides with high valence such as  $\text{Cu}^{3+}$  and  $\text{Fe}^{4+}$  [21]. The present system is the first example of transition-metal sulfide with negative charge-transfer energy. The negative charge-transfer energy indicates that the ground state has strong S  $3p$  hole character. Although the symmetry of the ground state is  ${}^3A_{2g}$ , the magnitude of the local spin at the Ni site is reduced to 0.55 in comparison with the ionic value  $S = 1$  by the strong Ni  $3d$ -S  $3p$  hybridization. In this sense, the  ${}^3A_{2g}$  state with the  $d^9L$  character is a triplet analogue of the Zhang-Rice singlet in high-Tc cuprates.

In Fig. 4, the valence-band spectrum is plotted with the line spectrum obtained by the  $\text{NiS}_6$  cluster model calculation with the parameters obtained from the Ni  $2p$  spectrum. Although the contribution from the GaS layer prevents us from fitting the valence-band spectrum, the overall agreement between the line spectrum and the valence-band spectrum support the cluster-model analysis of the Ni  $2p$  spectrum. The first ionization state has the

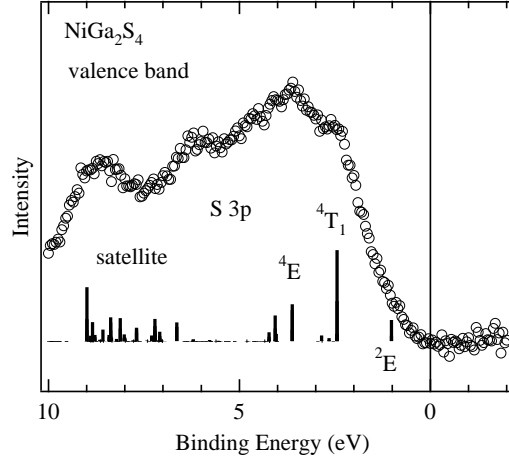


FIG. 4: Valence-band XPS of  $\text{NiGa}_2\text{S}_4$  (open circles). The line spectrum is obtained by the  $\text{NiS}_6$  cluster model calculation.

symmetry of  ${}^2E_g$  and the second ionization state is  ${}^4T_{1g}$ . This situation is similar to those of  $\text{NiS}$  and  $\text{NiS}_2$  which have small but positive charge-transfer energy [23, 24]. The excitation from the  ${}^3A_{2g}$  ground state to the  ${}^2E_g$  first ionization state is obtained by removal of an  $e_g$  electron. The  ${}^2E_g$  state is expected to have some energy-momentum dispersion due to the interaction between the  $\text{NiS}_6$  clusters and to form the  $e_g$  band.

In the next step, let us examine superexchange pathways in  $\text{NiGa}_2\text{S}_4$  based on the electronic structure parameters obtained from the analysis of the Ni  $2p$  spectrum. Since the  $t_{2g}$  orbitals are fully occupied and the neighboring Ni-S bonds are approximately orthogonal to each other in the two  $\text{NiS}_6$  clusters sharing their edges, the cell perturbation calculation [25] becomes rather simple and the superexchange interaction between the two clusters is given by the second order perturbation of S  $3p$ - $3p$  transfer term. In the  $\text{NiS}_6$  cluster, the exact ground state is given by  $\Psi_g({}^3A_{2g}) = \alpha|d^8({}^3A_{2g})\rangle + \beta|d^9L({}^3A_{2g})\rangle + \gamma|d^{10}L^2({}^3A_{2g})\rangle$ . Here, the  $\text{NiS}_6$  cluster is assumed to be a cubic octahedron in the calculation although it has a slight trigonal distortion in  $\text{NiGa}_2\text{S}_4$ . Since the S  $3p$  hole denoted as  $L$  is dominated by the  $3p_\sigma$  orbitals pointing to the Ni sites, it is reasonable to approximate that

$$|d^9L({}^3A_{2g})\rangle = \frac{1}{\sqrt{2}}(|d_{x^2-y^2}L_{3z^2-r^2}| + |L_{x^2-y^2}d_{3z^2-r^2}|). \quad (2)$$

Here,  $d_{x^2-y^2}$  and  $d_{3z^2-r^2}$  denote a hole in Ni  $3d$   $x^2 - y^2$  and  $3z^2 - r^2$  orbitals, respectively. The  $x$ -,  $y$ -, and  $z$ -axes are along the Ni-S bonds as shown in Fig. 5(a). The  $x^2 - y^2$  type S  $3p$

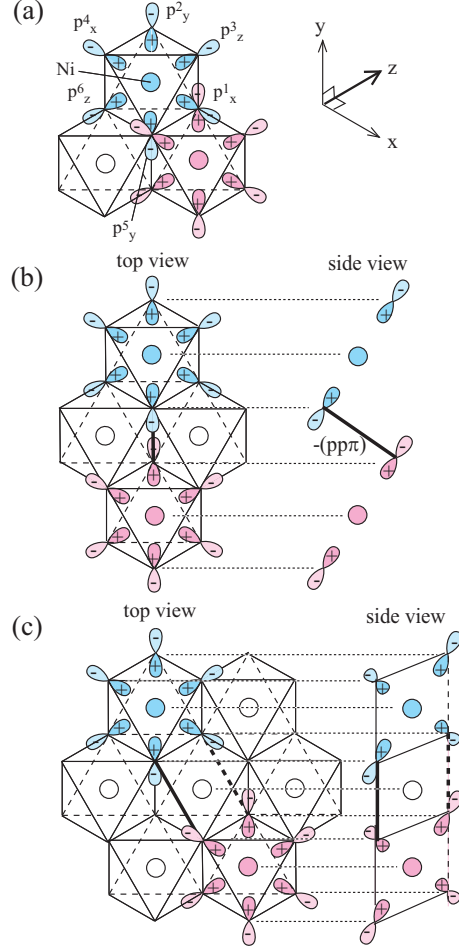


FIG. 5: (Color online) (a) Top view of the nearest neighbor clusters in the NiS<sub>2</sub> layer. (b) Top and side views for superexchange pathway between the second nearest neighbor clusters, which is given by the S 3*p*-3*p* transfer of  $-(pp\pi)$ , as indicated by the thick solid line. (c) Top and side views for two superexchange pathways between the third nearest neighbor clusters, which are given by the S 3*p*-3*p* transfer of  $[-(pp\sigma) + (pp\pi)]/\sqrt{2}$ , as indicated by the thick solid and broken lines.

molecular orbital is given by  $L_{x^2-y^2} = \frac{1}{2}(p_x^1 - p_y^2 + p_x^4 - p_y^5)$ , in which  $p_x^1$ ,  $p_y^2$ ,  $p_x^4$ , and  $p_y^5$  are  $p_x$  and  $p_y$  orbitals pointing to the Ni site [see Fig. 5(a)]. The  $d_{3z^2-r^2}$  type S 3*p* molecular orbital is given by  $L_{3z^2-r^2} = \frac{1}{\sqrt{3}}(p_z^3 + p_z^6) - \frac{1}{2\sqrt{3}}(p_x^1 + p_y^2 + p_x^4 + p_y^5)$ , in which  $p_z^3$  and  $p_z^6$  are  $p_z$  orbitals pointing to the Ni site. As a consequence, the overlap integral between the neighboring  $d^9L$  states with  ${}^3A_{2g}$  symmetry can be neglected. The superexchange pathways between the neighboring  $d^9L({}^3A_{2g})$  states are given by the transfer terms between the two S 3*p* molecular orbitals with  $L_{x^2-y^2}$  and  $L_{3z^2-r^2}$ . The transfer integrals between the neighboring

$L_{x^2-y^2}$  orbitals is  $\frac{1}{4}[(pp\sigma) + (pp\pi)]$  and that between the neighboring  $L_{3z^2-r^2}$  orbitals is  $\frac{1}{12}[(pp\sigma) + 9(pp\pi)]$ , where  $(pp\sigma)$  and  $(pp\pi)$  are the S  $3p$ - $3p$  transfer integrals. Therefore, the antiferromagnetic superexchange interaction between the neighboring sites is given by

$$J_1^{AF} = -\frac{\beta^2}{2U_p} \left\{ \frac{1}{16} [(pp\sigma) + (pp\pi)]^2 + \frac{1}{144} [(pp\sigma) + 9(pp\pi)]^2 \right\}, \quad (3)$$

where  $U_p$  is the Coulomb interaction between the S  $3p$  holes at the same S sites and is expected to be  $\sim 1$  eV [26]. Since  $\beta^2 = 0.6$ ,  $(pp\sigma) = 0.6$  eV, and  $(pp\pi) = -0.15$  eV,  $J_1^{AF} \sim -5$  meV. On the other hand, the two S  $3p$  holes at the shared sulfur sites have Hund coupling due to the on-site exchange integral  $J_p$  at the S site. The ferromagnetic interaction due to the Hund coupling is given by  $J_1^F = \frac{\beta^4}{18} J_p \sim 4$  meV, where  $J_p$  is the Hund coupling between the S  $3p$  holes at the same S sites and is assumed to be  $\sim 0.2$  eV. As a result, the total magnetic interaction between the neighboring sites  $J_1 = J_1^{AF} + J_1^F$  is estimate to be  $\sim -1$  meV. The transfer integral between the second neighbor  $L_{x^2-y^2}$  orbitals is given by  $-\frac{1}{3}(pp\pi)$  and that between the second neighbor  $L_{3z^2-r^2}$  orbitals can be neglected [see Fig. 5 (b)]. The superexchange interaction  $J_2$  due to the transfer term between the second neighbor  $d^9L$  states becomes

$$J_2 = -\frac{\beta^2}{18U_p} (pp\pi)^2, \quad (4)$$

which is  $\sim -1$  meV and as small as  $J_1$ .

In contrast, the transfer integral between the third neighbor  $L_{x^2-y^2}$  orbitals is  $\frac{1}{4}[(pp\sigma) - (pp\pi)]$  and that between the third neighboring  $L_{3z^2-r^2}$  orbitals is  $\frac{1}{4\sqrt{3}}[-(pp\sigma) + (pp\pi)]$  as shown in Fig. 5 (c). The superexchange interaction  $J_3$  between the third neighbor sites due to the transfer term between the  $d^9L$  states is given by

$$J_3 = -\frac{\beta^2}{24U_p} [(pp\sigma) - (pp\pi)]^2, \quad (5)$$

which is estimated to be  $\sim -14$  meV. The superexchange interaction between the forth neighbor sites is beyond the second order perturbation on the  $p$ - $p$  transfer integrals  $(pp\sigma)$  and  $(pp\pi)$ , and is expected to be negligibly small. The present cell perturbation analysis predicts that the third neighbor superexchange interaction is dominant consistent with the neutron diffraction result [14].

In conclusion, the electronic structure of  $\text{NiGa}_2\text{S}_4$  with the  $\text{NiS}_2$  triangular lattice is investigated using photoemission experiment and model calculations. The Ni  $2p$  photoemission data and the cluster model calculation show that the ground state has the  $d^9L$  character ( $L$



is a S  $3p$  hole) which is a triplet analogue of the Zhang-Rice singlet state. The strong S  $3p$  hole character of the ground state provides the enhanced superexchange interaction between the third nearest neighbor sites.  $\text{NiGa}_2\text{S}_4$  is a unique spin-disordered system in that the negative charge-transfer energy allows unexpectedly long superexchange pathways.

This work was supported by Grant-In-Aid from Ministry of Education, Culture, Sports, Science and Technology of Japan.

- 
- [1] R. Moessner, *Can. J. Phys.* **79**, 1283 (2001).
  - [2] H. F. Pen, J. van den Brink, D. I. Khomskii, and G. A. Sawatzky, *Phys. Rev. Lett.* **78**, 1323 (1997)
  - [3] S.-H. Lee, D. Louca, H. Ueda, S. Park, T. J. Sato, M. Isobe, Y. Ueda, S. Rosenkranz, P. Zschack, J. Iniguez, Y. Qiu, and R. Osborn, *Phys. Rev. Lett.* **93**, 156407 (2004).
  - [4] Y. Motome and H. Tsunetsugu, *Phys. Rev. B* **70**, 184427 (2004).
  - [5] M. Schmidt, W. Ratcliff II, P. G. Radaelli, K. Refson, N. M. Harrison, and S. W. Cheong, *Phys. Rev. Lett.* **92**, 056402 (2004).
  - [6] D. I. Khomskii and T. Mizokawa, *Phys. Rev. Lett.* **94**, 156402 (2005).
  - [7] S.-H. Lee, C. Broholm, T. H. Kim, W. Ratcliff II, and S.-W. Cheong, *Phys. Rev. Lett.* **84**, 3718 (2000).
  - [8] Y. Yamashita and K. Ueda, *Phys. Rev. Lett.* **85**, 4960 (2000).
  - [9] O. Tchernyshyov, R. Moessner, and S. L. Sondhi, *Phys. Rev. Lett.* **88**, 067203 (2002);
  - [10] A. P. Ramirez, G. P. Espinosa, and A. S. Cooper, *Phys. Rev. Lett.* **64**, 2070 (1990).
  - [11] R. Moessner and S. L. Sondhi, *Phys. Rev. Lett.* **86**, 1881 (2001).
  - [12] B. Canals and C. Lacroix, *Phys. Rev. Lett.* **80**, 2933 (1998).
  - [13] Y. Shimizu, K. Miyagawa, K. Kanoda, M. Maesato, and G. Saito, *Phys. Rev. Lett.* **91**, 107001 (2003).
  - [14] S. Nakatsuji, Y. Nambu, H. Tonomura, O. Sakai, S. Jonas, C. Broholm, H. Tsunetsugu, Y. Qiu, and Y. Maeno, *Science* **309**, 1697 (2005).
  - [15] S. Fujimoto, *Phys. Rev. B* **73**, 184401 (2006).
  - [16] K. Onuma, Y. Nambu, S. Nakatsuji, O. Sakai, Y. Maeno, in preparation.
  - [17] M. A. van Veenendaal and G. A. Sawatzky, *Phys. Rev. Lett.* **70**, 2459 (1993).

- [18] F. M. F. de Groot, J. C. Fuggle, B. T. Tole, and G. A. Sawatzky, *Phys. Rev. B* **42**, 5459 (1990).
- [19] A.E. Bocquet, T. Mizokawa, T. Saitoh, H. Namatame, and A. Fujimori, *Phys. Rev. B* **46**, 3771 (1992).
- [20] K. Okada and A. Kotani, *J. Phys. Soc. Jpn.* **58**, 2578 (1989).
- [21] T. Mizokawa, H. Namatame, A. Fujimori, K. Akeyama, H. Kondoh, H. Kuroda, and N. Kosugi, *Phys. Rev. Lett.* **67**, 1638 (1991).
- [22] D. D. Sarma, H. R. Krishnamurthy, S. Nimbkar, S. Ramasesha, P. P. Mitra, and T. V. Ramakrishnan, *Pramana (J. Phys.)* **38**, L531 (1992).
- [23] S. R. Krishnakumar and D. D. Sarma, *Phys. Rev. B* **68**, 155110 (2003).
- [24] S. R. Krishnakumar, N. Shanthi, and D. D. Sarma, *Phys. Rev. B* **66**, 115105 (2002).
- [25] J. H. Jefferson, H. Eskes, and L. F. Feiner, *Phys. Rev. B* **45**, 7959 (1992).
- [26] H. Eskes and J. H. Jefferson, *Phys. Rev. B* **48**, 9788 (1993).